

PCCP

Accepted Manuscript



This is an *Accepted Manuscript*, which has been through the Royal Society of Chemistry peer review process and has been accepted for publication.

Accepted Manuscripts are published online shortly after acceptance, before technical editing, formatting and proof reading. Using this free service, authors can make their results available to the community, in citable form, before we publish the edited article. We will replace this *Accepted Manuscript* with the edited and formatted *Advance Article* as soon as it is available.

You can find more information about *Accepted Manuscripts* in the [Information for Authors](#).

Please note that technical editing may introduce minor changes to the text and/or graphics, which may alter content. The journal's standard [Terms & Conditions](#) and the [Ethical guidelines](#) still apply. In no event shall the Royal Society of Chemistry be held responsible for any errors or omissions in this *Accepted Manuscript* or any consequences arising from the use of any information it contains.

ARTICLE

Electronic and Optical Properties of Polypyridylruthenium Derivatized Polystyrenes: Multi-level Computational Analysis of Metallo-Polymeric Chromophore Assemblies

Cite this: DOI: 10.1039/x0xx00000x

Received 00th January 2012,
Accepted 00th January 2012

DOI: 10.1039/x0xx00000x

www.rsc.org/

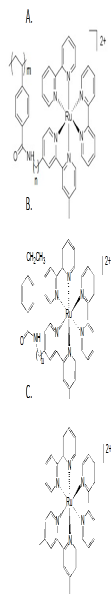
Zoe Watson,^a Shahar Keinan,^{a,*} and Yosuke Kanai^{a,b *}

Great effort is geared toward investigation of new materials for solar energy conversion in recent years. Polymeric chromophore assemblies consisting of $[\text{Ru}(\text{bpy})_3]^{2+}$ complexes attached to a polystyrene backbone have gained considerable interest in recent years because of their structural flexibility combined with their ability to efficiently capture solar energy and transport the captured energy in the form of exciton or charges. We employ a combination of computational methods to examine how opto-electronic properties of $[\text{Ru}(\text{bpy})_3]^{2+}$ complexes are influenced by the polymer dynamics in these polymeric chromophore assemblies. The covalent linker between the polymer and the light-absorbing Ru complex is thought to play an important role in optimizing the assemblies for solar energy conversion and transport. We find that the presence of $-\text{CH}_2-$ groups in the linker has a significant impact on the Highest Occupied Molecular Orbital (HOMO) and Lowest Unoccupied Molecular Orbital (LUMO) energies of the pendants. Generally speaking, a longer linker leads to higher HOMO energies. Without the presence of $-\text{CH}_2-$ groups, a mixture of *cis* and *trans* amide bond in the covalent linker leads to a bimodal distribution for both HOMO and LUMO energies. Importantly, we find that distributions of orbital energies from individual $[\text{Ru}(\text{bpy})_3]^{2+}$ pendants have the maximum overlap when there is only one $-\text{CH}_2-$ group in the linker. Such an isotropic energy distribution is likely to be important for charge transport within the assemblies. We also find that in contrast to the isolated $[\text{Ru}(\text{bpy})_3]^{2+}$ complex, the HOMO is generally found on the linker rather than on Ru atom. This does not change the character of the metal-to-ligand charge transfer (MLCT) excited states, as these excitations in the pendants do not derive from HOMO/LUMO transitions but rather from HOMO-2/LUMO transition since HOMO-2 is located on the Ru atom.

Introduction

Solar energy conversion is one of the most pressing societal challenges today.^{1 2 3 4 5} Solar-to-fuel processes convert solar energy into chemical energy through a series of redox reactions.⁶ Many groups have been working on this highly challenging problem of reducing CO_2 or water molecules to useful fuels (e.g. CH_4 and H_2) while oxidizing water to O_2 .⁷ However, the reaction kinetics and the number of electrons involved in these catalytic processes require a means to capture sparse solar photons and funnel the captured excitation energies (excitons) and/or charges to the catalytic centers as in natural photosynthesis.⁸ When the molecular chromophores are used as in the Dye Sensitized Photoelectrosynthesis Cells (DSPEC) solar-fuel approach, assembling a large number of chromophores such that the excitons can be efficiently generated and charges are transported to the reaction center is important. Covalently linking the chromophores to the polymeric materials is an attractive approach since it offers a structurally flexible motif that can be attached to various solid-state surfaces and also to other catalytic molecules.⁹

Indeed, polymeric chromophore assemblies containing transition metal complexes have received considerable attention in recent years as a new class of functional and flexible materials for potential applications in photorefractivity, catalysis, and photovoltaics. Chemically incorporating photo-active transition metal complexes as chromophores onto a polymer backbone is a highly promising approach to combine the photo-active properties of various organometallic systems with electron/energy transport properties of flexible polymeric materials. Several groups have been working on the synthesis of these novel materials based on d-6 transition metal (TM) complexes such as $[\text{Ru}(\text{bpy})_3]^{2+}$, and the covalent linkage of the TM complexes to the polymer appears to be ideal in preventing the aggregation of the TM complexes. Representative systems of polystyrene tethered to d-6 TM complexes with ether or amide linkages have been recently investigated experimentally.⁹ In particular, intrinsic energy and electron transport within these metallo-polymers were investigated for their use as a flexible electron/energy transport material in solar-fuel systems.¹⁰ ¹¹ These experimental works have provided some key insights into



Scheme 1. The structures of the molecules studied in this manuscript.

A. Polymer **n0** has $n=0$, polymer **n1** has $n=1$ ($-\text{CH}_2-$ group) and polymer **n2** has $n=2$ ($-\text{CH}_2\text{CH}_2-$ group). All of the polymers studied were of length $m=20$. **B.** Pendant with linker. **C.** Pendant without the linker.

the mechanism and dynamics of exciton and charge transport within the polymer assemblies, featuring long-lived triplet metal-to-ligand charge transfer (MLCT) excited states (excitons) in the TM complexes.^{11, 8} In the metallo-polymeric systems with ruthenium (II) polypyridine pendant moieties in particular, fast energy transfer via MLCT excitons hopping from site-to-site has been observed in a time scale of nanoseconds.¹² These experimental studies indicated that photophysical and electron/energy transport properties of these polymeric chromophore assemblies depend on various structural details strongly (such as the relative spatial arrangement between the Ru (II) units).⁹

In order to make progress in this area, improved synthesis and detailed characterization of opto-electronic properties of these polymeric assemblies are necessary. Experimental preparation of metallo-polymer polystyrene derivatives through amide coupling chemistry has been reported in literature.⁹ A methyl-amide-carbonyl linker was used to covalently connect the polystyrene backbone and the pendant polypyridyl complexes of Ru(II). A recent work introduced the Atom Transfer Radical Polymerization (ATRP) approach as a novel synthesis method, ensuring small polymer dispersity indices and controlled chain lengths. Using this methodology, $[\text{Ru}(\text{II})(\text{bpy})_2(\text{CH}_3\text{-bpy-CH}_2\text{NH}_2)]$ (bpy = 2,2'-bipyridine and $\text{CH}_3\text{-bpy-CH}_2\text{NH}_2$ = 4-methyl-4'-aminomethyl-2,2'-bipyridine) complexes were attached controllably to each polystyrene repeat unit, resulting in the polymer shown in Scheme 1.

In order to make systematic progress in tailoring the polymeric chromophore assemblies for various opto-electronic applications, detailed understanding of relationships between photo-physical properties and the polymer assembly structure is desired at the atomistic level. At the same time, investigating

such a highly complex system presents a challenge for computational modelling based on electronic structure theory because of its large size and statistically diverse conformations. In this work, we use a multi-scale computational strategy of synergistically employing ab-initio/semi-empirical quantum mechanical calculations and classical molecular dynamics simulations for the investigation. In particular, the question of how opto-electronic properties of individual transition metal complexes are influenced by the polymer dynamics and covalent linkages is addressed in context of their role in photo-absorption and electron/energy transport. To this end, we computationally explore several polymers derivatized by carboxyl coupling to a polypyridyl Ru(II) complex. In our previous work, Molecular Dynamics (MD) simulations were performed to generate a large ensemble of these statistically complex polymeric materials. The results of these simulations were used for analysis of nearest-neighbour Ru-Ru distances for each polymer at 90% and 100% loading of the chromophores on the polymer backbone.⁹ The Ru-Ru distance was found not to vary significantly with the linker lengths or loading level of the chromophores. In this work, using the same MD trajectories, electronic structure calculations are used to examine key electronic states (i.e. Highest Occupied Molecular Orbitals (HOMO) and Lowest Unoccupied Molecular Orbitals (LUMO)) as well as the excitation energies for individual TM complexes attached to the polymers, in order to gain insight into the importance of the polymer dynamics on the electronic structure of the TM complexes that are responsible for the energy/energy transfer. In particular, we address to what extent the dynamics influences the heterogeneity of optoelectronic properties among the TM complexes as a function of the covalent linkage to the polymer backbone. The methodology we employ here has been used before; for example, Beratan and co-workers have studied electron transfer in DNA using MD simulations, followed by INDO/s calculations on snapshots.^{13, 14} Also, MacKenzie et al. studied thin films of fullerene derivatives using MD simulations, followed by DFT calculations and Monte Carlo methods to calculate electron mobility.^{MacKenzie, 2010 #18} The same approach was also used by Tummala et al. for studying solvent and temperature effects on PCMB polymers.¹⁵

Methods

A detailed description of how we obtained the geometries used here has already been published.⁹ Here we only describe the methodology used in broader terms:

Polymer Geometries

Polymer structures were calculated using MD simulations in the MaterialsStudio Forcite module (Accelrys Software Inc., San Diego, 2011). The force fields parameters for the Universal Force Field (UFF)¹⁶ were based on DFT-optimized geometries. The geometry of each pendant ($[\text{Ru}(\text{bpy})_3]^{2+}$ complex with the linker) was optimized using Density Functional Theory (DFT) calculations with B3LYP exchange-correlation functional¹⁷ and Lan12DZ Gaussian basis sets^{18, 19, 18} using Gaussian09.²⁰

Geometries of the polymers with 20 pendant units were constructed for the simulations. Then, the simulation cell was prepared by including the polymer, PF_6^- (counter ions), and acetonitrile (solvent). The size of the simulation cell was determined so that the polymer is separated by its own image of the periodic boundary conditions by at least 15 Å of "solvent wall" in each direction. The simulation cell

was first annealed, and then the MD simulation was performed. During the MD simulations, snapshots of the trajectories were collected every 0.5 ps during the second ns of the MD simulation, collecting 2000 snapshots for further analysis of their electronic structure. With 20 pendant units in each polymer and 2000 snapshots obtained from each MD simulation, a total of 40,000 different $[\text{Ru}(\text{bpy})_3]^{2+}$ complex configurations were obtained for each polymer for further analysis with electronic structure calculations.

Electronic Structure Calculations for Electronic Energy Levels and Excited States

Atomic coordinates of each pendant were extracted and the truncated σ bonds were each capped with a hydrogen atom. For each pendant unit we considered two structures - the entire $[\text{Ru}(\text{bpy})_3]^{2+}$ complex with the linker and only the $[\text{Ru}(\text{bpy})_3]^{2+}$ without the linker, Scheme 1, B and C. Semi-empirical electronic structure calculations based on model Hamiltonian with screened Intermediate Neglect of Differential Overlap/Screened Approximation (INDO/S),²¹ as implemented in the CNDO program,^{22, 22} were then performed for the 40,000 pendant geometries for each polymer, to obtain statistically converged distributions of electronic energy levels. For comparison, single-point DFT calculations were performed on select configurations to validate the semi-empirical electronic structure calculations (See Supporting Information, Fig. S11). These Density Functional Theory (DFT) calculations used the B3LYP exchange-correlation functional¹⁷ and LanL2DZ Gaussian basis sets^{18, 19, 18} using Gaussian09.²⁰ Excited state properties (e.g. optical energy gap, optical absorption spectrum) were then calculated by including electron-hole pair interaction at Configuration Interaction Singles (CIS) level of theory with the molecular orbitals obtained with the INDO/S Hamiltonian. The INDO/S method has been shown previously to reproduce DFT and Time-dependent-DFT calculations for $[\text{Ru}(\text{bpy})_3]^{2+}$ complex and other Ru diimine complexes.^{23, 24}

Results and Discussion

We have previously used our MD simulation to show that for these polymers, shorter linkers resulted in average shorter average Ru-Ru distance between pendants, which was in agreement with

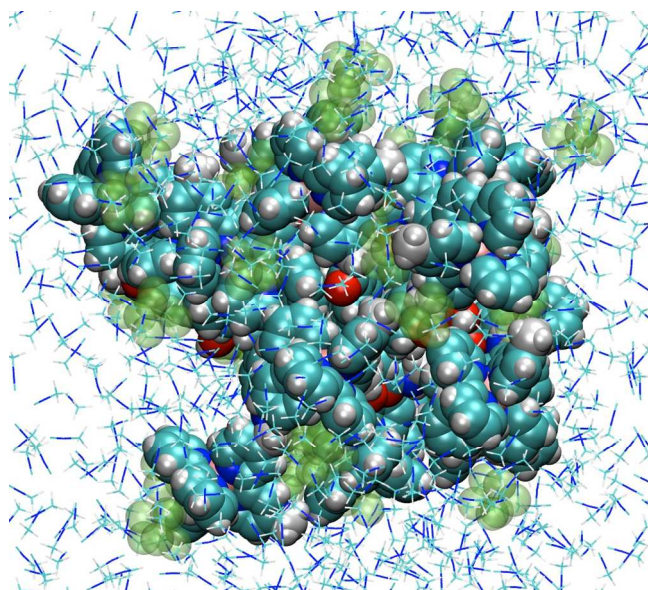


Figure 1. A representative snapshot from MD simulation of **n1**. The polymer is shown using vDW spheres (White for hydrogen atoms, red for oxygen atoms, grey for carbon atoms), PF_6^- counter ions are shown as green vDW spheres, and the solvent is shown in a stick representation.

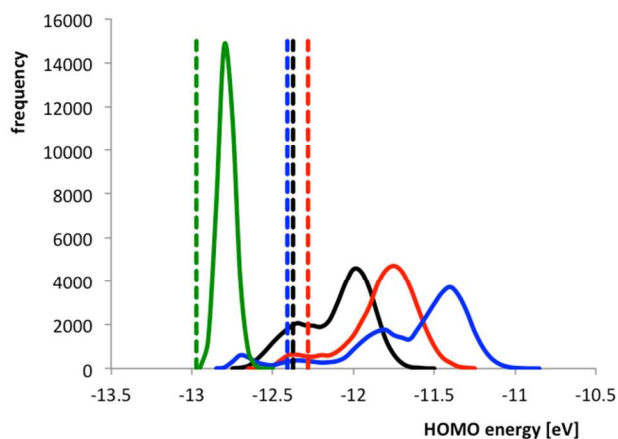


Figure 2. HOMO energy distributions from 40,000 pendant structures obtained from 2,000 MD snapshots for each polymer. Black line is for pendants from the **n0** polymer, red line is for pendants from the **n1** polymer, and blue line is for pendants from the **n2** polymer. The green line is the energy distributions from pendants from the **n1** polymer, without the linker. This is to show $[\text{Ru}(\text{Bpy})_3]^{2+}$ behaviour in the same environment. For comparison we also show the INDO/S HOMO energy of geometry-optimized $[\text{Ru}(\text{Bpy})_3]^{2+}$ using DFT in green dashed line, **n0** monomer, black dashed line, **n1** monomer, red dashed line and **n2** monomer, blue dashed line.

experimental results.⁹ Fig. 1 shows a representative snapshot of the **n1** polymer from the MD simulation. Here, we investigate how optoelectronic properties of individual $[\text{Ru}(\text{bpy})_3]^{2+}$ pendants are influenced by the polymer dynamics in these assemblies.

Frontier Orbitals Energy Distribution

From the trajectories of the MD simulations, we obtained, for each of the 3 polymers, 2000 snapshots, each with 20 pendants, totalling 40,000 different $[\text{Ru}(\text{bpy})_3]^{2+}$ complex configurations for each polymer. We then calculated the electronic structure for each configuration with the INDO/s semi-empirical Hamiltonian. Fig. 2 shows the HOMO energy distribution for the pendant structures in the three polymers we considered here as well as for the individual pendant structures whose geometries were optimized using DFT calculations. The difference in the HOMO energy distribution among the three ensembles with the different linker groups (**n0**, **n1**, and **n2**) derives from the varying linker length. The energy distribution for the linker-less pendant is also shown in Fig.2 in the green line, to differentiate between the environment and linker's influence on the HOMO. We found that the energy distributions for the linker-less pendants are visually identical for the three polymers, and thus only one distribution is shown in the green line. Generally, the HOMO energy distribution for the ensembles is found to shift higher in energy as the linker length increases. The HOMO energy is expected to increase (become less stable) as the structures deviate from ideal geometry and become more distorted. As can be expected, the Ru-localized HOMO of the *isolated* $[\text{Ru}(\text{Bpy})_3]^{2+}$ complex is consistently near the bottom of the HOMO energy distribution for all the ensembles.

Fig. 3 shows the equivalent set of energy distributions as in Fig.2 but for the LUMO. Unlike the HOMO energy distributions, the LUMO energies distributions are quite similar for the pendants in all three polymers. Interestingly, both **n1** and **n2** equilibrium structures have a higher LUMO energy than the LUMO energy distribution obtained for the ensembles, which is the opposite of what we found for the HOMO energy. The LUMO energy for the equilibrium structure (shortest-linker pendant) is located in the center of the LUMO energy distribution for **n0**

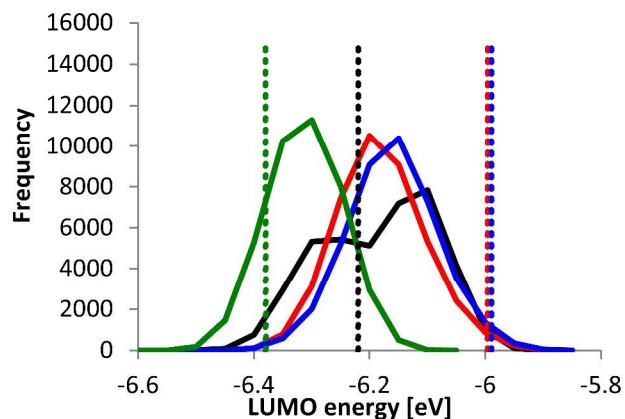


Figure 3. LUMO energy distributions from 40,000 pendant structures obtained from 2,000 MD snapshots for each polymer. Black line is for pendants from the **n0** polymer, red line is for pendants from the **n1** polymer, and blue line is for pendants from the **n2** polymer. The green line is the energy distributions from pendants from the **n1** polymer, without the linker. For comparison we also show the INDO/S LUMO energy of the DFT (B3LYP/Lan12DZ) optimized geometry of the $[\text{Ru}(\text{Bpy})_3]^{2+}$, green dashed line, **n0** monomer, black dashed line, **n1** monomer, red dashed line and **n2** monomer, blue dashed line.

polymer. We also note that **n0** is the only case in which a bimodal distribution is observed for the LUMO energy distribution as shown in Fig. 3.

These frontier orbitals (i.e. HOMO and LUMO) are of particular importance because they represent the energetically most stable states for a hole and an electron, respectively. For comparison, we calculated the electronic structure of an isolated, symmetrical $[\text{Ru}(\text{Bpy})_3]^{2+}$ molecule. From our calculation and previous studies, it is well known that the HOMO is located on the Ru atom in the isolated $[\text{Ru}(\text{bpy})_3]^{2+}$ unit while the LUMO is usually located on the bpy ligands.¹² Contrary to the case of the isolated $[\text{Ru}(\text{Bpy})_3]^{2+}$, we find in this study that the HOMO is mostly located on the linker group in the Ru-complex pendants. The spatial characteristics of the LUMO are similar to that of isolated $[\text{Ru}(\text{Bpy})_3]^{2+}$. Due to the structural symmetry of the isolated molecule, the LUMO is distributed between the three identical bpy ligands. However, in the polymeric, un-symmetrical system we find that the LUMO is more localized, residing mostly on one or two bpy ligands of the Ru complex in the pendant. The HOMO-1 state also shows the same qualitative spatial characteristics as the HOMO. The HOMO-2 state is the highest occupied state that is localized on Ru atom in over 90% of the configurations as discussed in detail later. Both INDO/S and DFT results show the same spatial character for these frontier orbitals (See Supporting Information, Fig. S11, S12).

The LUMO is located on the bpy ligand, which is the same for all three polymers, and would not explain the difference in the LUMO energy distribution between the three polymers, particularly the bimodal distribution for **n0**. To understand this observation, distributions of several geometric parameters in the ensemble were analysed, and we found that the separation distance between the

oxygen atom in the linker group and the Ru atom yields an interesting characteristic among the three polymers as shown in Fig 4.

For both the **n1** and **n2** polymers, the equilibrium pendant structure has a much shorter Ru-O distance (5.5 Å and 5.2 Å for the **n1** and **n2**, respectively, equilibrium pendants) than those of the ensembles, Fig. 4. This is because the linker group is able to wrap close to the $[\text{Ru}(\text{bpy})_3]^{2+}$ unit in the equilibrium structures as shown in the inset of Fig. 4. In contrast, the dynamical polymer motion causes the linker group to be extended away from the $[\text{Ru}(\text{bpy})_3]^{2+}$ unit due to the steric hindrance for the ensemble. Note that the close proximity of the linker group to the bpy ligands destabilizes the LUMO state, which is localized on the ligands. For the **n0** polymer, where there is no extra methylene bridge in the linker, we found that the equilibrium structure shows the linker extended away from the $[\text{Ru}(\text{bpy})_3]^{2+}$ unit. The Ru-O distribution for the ensemble shows a bimodal distribution just as for the LUMO energy distribution. We find that these two distinct peaks are present in the distribution because the pendants fall into two groups: those for which the amide bond is *cis*, and those for which the bond is *trans* (See Supporting Information, Fig. S13). For each polymer, all of the pendants began in the same configuration, but they were able to change between *cis* and *trans* during the annealing step.

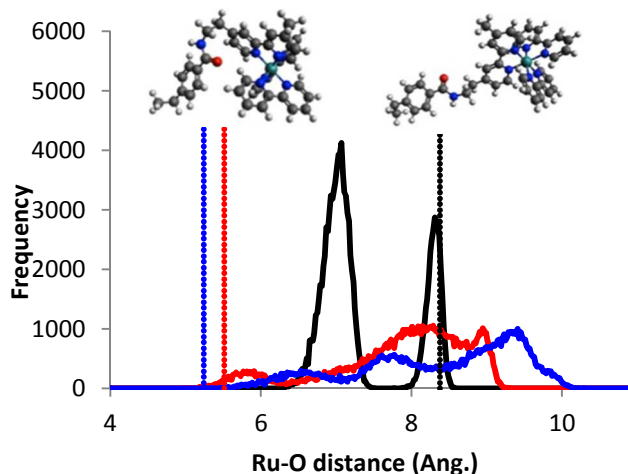


Figure 4. The distance between Ru and Oxygen atoms from 40,000 pendant structures obtained from 2,000 MD snapshots for each polymer. We also show (left top) the geometry of the ideal **n2** monomer and (top right) the geometry of representative **n2** monomer taken from MD snapshot. Black line is for pendants from the **n0** polymer, red line is for pendants from the **n1** polymer, and blue line is for pendants from the **n2** polymer. For comparison we also show Ru-O distance for the DFT (B3LYP/Lan12DZ) optimized geometry of the **n0** monomer, black dashed line, **n1** monomer, red dashed line and **n2** monomer, blue dashed line.

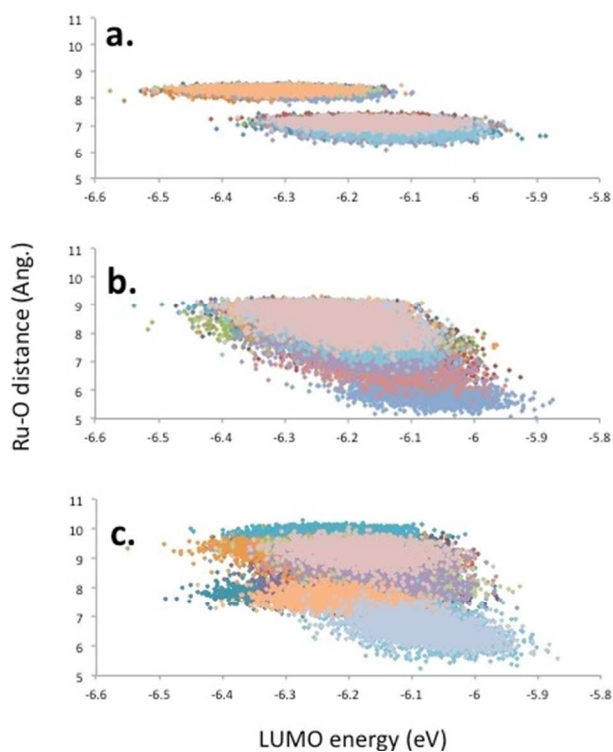


Figure 5. Plot of the Ru-O distances for each pendant vs. the LUMO energy for a. **n0**, b. **n1** and c. **n2**. The values are color coded for each pendant.

In order to further understand how the frontier orbital energies are influenced by the polymer dynamics, the Ru-O distances are plotted against both the HOMO energy (Fig. 6) and the LUMO (Fig. 5) energy for individual pendant structures, colored differently for each pendant. For the **n0** polymer, Fig. 5a shows two distinct distributions, similar to our observations in Fig. 3 and Fig. 4. All of the pendant structures belong to either of the two regions but not to both, corresponding to whether the amide bond is *cis* or *trans*. Interestingly; there are no significant changes in the Ru-O distance for individual pendant structures, although HOMO and LUMO energies change considerably. In the case of the **n1** and **n2** polymers, however, there is no bimodal distribution of the distances and energies as is the case for **n0**. At the same time, we observe a general trend of having higher HOMO energies for longer Ru-O distances, and each pendant structure yields a rather distinct energy range of ~ 0.5 eV. The broad distributions for Ru-O distance are mainly due to the fact that the Ru complex is able to move around more freely for **n1** and **n2** polymers because of $-\text{CH}_2-$ groups present in the linker. We also observe that each pendant structure shows a HOMO energy distribution that is more scattered for **n2** polymer than for **n1** polymer. The correlation plots for **n1** and **n2** polymers also show a strong general trend of having lower LUMO energies for larger Ru-O distances.

It is tempting to fit the HOMO orbital energy distribution by several overlapping gaussians (See, for example, Supporting Information Fig. S14). For the **n2** pendants HOMO orbital energy distribution can be described by four overlapping gaussians. The four gaussians were fitted by hand to match the orbital energy distribution: one gaussian with the center located at 11.4eV (± 0.17 eV), another one with the center at 11.8eV

(± 0.21 eV), the third one (very small contribution) at -12.35eV and the last one at -12.7eV. However, the real picture is much more complicated and the HOMO energy distribution is a combination of multiple gaussians, each gaussian describing different pendant from **n0** (See Supporting Information, Fig. S15), **n1** (See Supporting Information, Fig. S16), and **n2** (See Supporting Information, Fig. S17). It can be seen that for most of the pendants the orbitals energy distribution can be described as gaussian with broadening of $\sim \pm 0.1$ - 0.2 eV. These are the same characteristics that previous works have found. For example, Beratan and co-workers have observed that the energy distributions of HOMO and LUMO orbitals in DNA segments can be described as a gaussian with broadening to be around ± 0.1 eV.¹³ Troisi et al. calculated broadening for frontier orbitals to be 0.05-0.1eV in thin films of P3HT.²⁵ This kind of behaviour is characteristic of orbitals that are located on a single site (For example, the Ru atom) and that are broadened by thermal fluctuations on that site. For lower orbitals, such as HOMO-2, HOMO-3 or HOMO-4, the orbitals are located on a single site, and thus are closer to a single gaussian (see Supporting Information for **n0**, Fig. S18; **n1**, Fig. S19; and **n2**, Fig. S110, also orbital plot for all monomers, Fig. S111).

Ru-centered states

The polymers described here are important as photon harvesting materials due to their long-distance exciton and charge-transport mechanisms through the $[\text{Ru}(\text{bpy})_3]^{2+}$ units. Ru-centered molecular states are thus of great interest because of the long-lived metal-to-ligand charge transfer (MLCT) excited states, and also for the hopping transport of a hole in Ru^{+3} oxidation state. In our calculations, the HOMO-2 state was found to be the Ru-centered electronic state that is closest to the energy gap, whereas HOMO and HOMO-1 states are

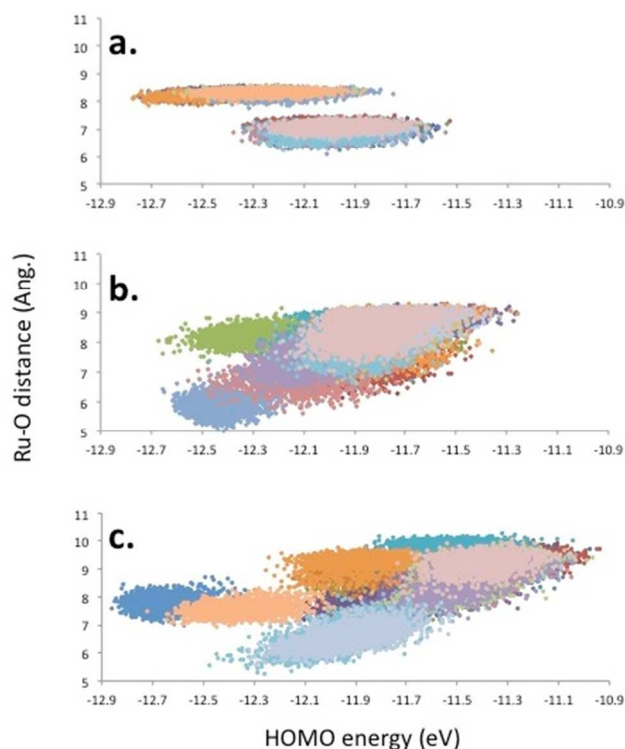


Figure 6. Plot of the Ru-O distances for each pendant vs. the HOMO energy for a. **n0**, b. **n1** and c. **n2**. The values are color coded for each pendant.

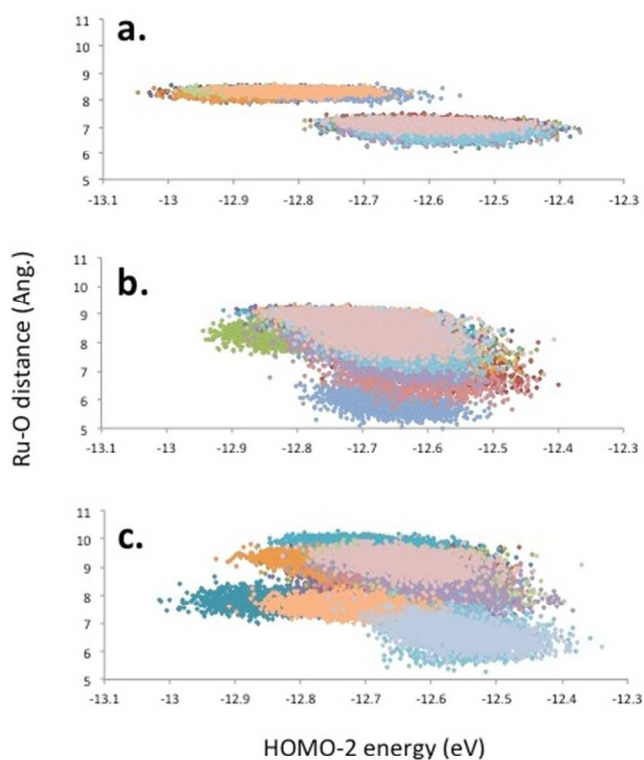


Figure 7. Plot of the Ru-O distances for each pendant vs. the HOMO-2 energy for a. **n0**, b. **n1** and c. **n2**. The values are color coded for each pendant.

both mostly localized on the linker group. In order to gain a better understanding of how the energy of these Ru-centered HOMO-2 states are influenced by the polymer dynamics, the Ru-O distance is plotted against HOMO-2 energy for individual pendants (**Fig. 7**). The correlation plot between HOMO-2 energy and the Ru-O distance generally shows that there are two distinct distributions for the **n0** polymer while we find very little or no correlation between Ru-O distance and Ru-centered HOMO-2 energy for the **n1** and **n2** polymers (unlike what we find for the HOMO). In the case of **n1** and **n2**, we attribute this weak correlation to the fact that the electronic state is localized on the Ru atom, and is less influenced by the closeness of the linker to the bpy ligands. For **n1** polymer, almost all of the pendants span the same Ru-O distance range and also the energy range of ~ 0.5 eV is quite uniform. These distributions appear to depend much more on the individual pendants for **n2** polymer.

Optical Excitation

For all individual Ru-complex pendants with and without the linker (total 40,000 structures per polymer) we calculated the excitation energies using CIS (with singlet excitation using 60 orbitals above and below HOMO) with the single-particle orbitals from INDO/S. **Fig. 9** shows the excitation energy distribution, which is obtained by counting the number of excitations for each wavelength in the ensemble of 40,000 structures. **Fig. 8** shows the optical absorption spectrum for the ensemble, which is obtained by summing the oscillator strength of all excitations at a given wavelength. This spectrum represents the thermally average optical absorption spectrum, which takes into account the fact that some

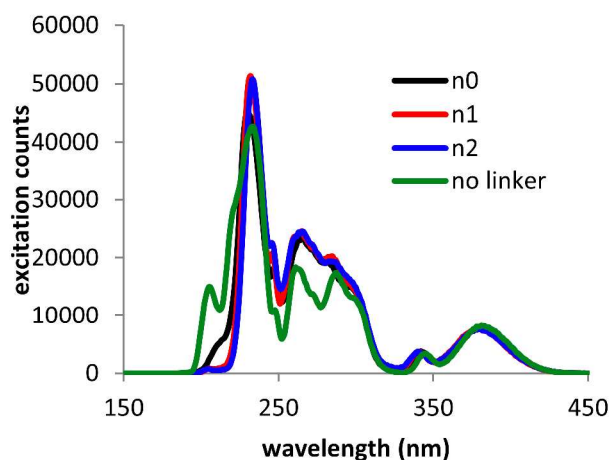


Figure 9. INDO/S excitation counts for the polymer containing **n0** pendant (black line), **n1** pendant (red line), and **n2** pendant (blue line) with linker and of **n0** pendant without linker (green line). For simplicity, only polymer containing the **n0** without the linker is shown, however, **n1** and **n2** results are similar.

transitions are not allowed (dark state). In **Fig. 8**, most of the peaks are independent of whether or not the linker group was included in the calculations, except for the sharp peak near 220 nm observed for the no-linker case. Similarly, in **Fig. 9** the strong peak of 205 nm is observed only when no linker is present. These peaks derive from a bpy $\pi \rightarrow$ bpy π^* transition, and our analysis shows that the covalent attachment of the linker to the bpy ring strongly perturbs these delocalized states on the bpy, resulting in the redshift when the linker is attached. Comparison of **Fig. 8** and **Fig. 9** shows that there exists a prominent dark state at 340 nm in all cases, which is apparently rather insensitive to dynamical fluctuations of the polymer assemblies.

The calculated absorption spectra are in good agreement with measured UV-VIS spectra for these polymers showing MLCT peak ($d\pi(\text{Ru}) \rightarrow \pi^*(\text{bpy})$) around 380 nm/3.27 eV (450 nm/2.76 eV in experiment) and broad $\pi \rightarrow \pi^*$ peaks at 220-320 nm.^{9, 12} Note that

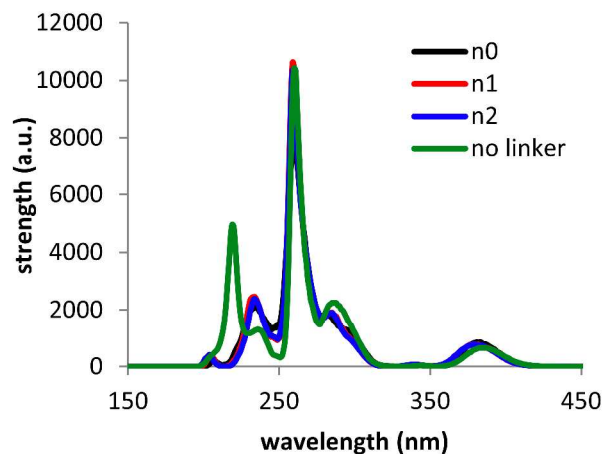


Figure 8. Sum of all calculated INDO/S electronic spectra for the polymer containing **n0** pendant (black line), **n1** pendant (red line), and **n2** pendant (blue line) with linker and of **n0** pendant without linker (green line). For simplicity, only polymer containing the **n0** without the linker is shown, however, **n1** and **n2** results are similar.

the MLCT peak can be rather sensitive to the specific solvent used in experiments.^{9,12} The spatial character of these peaks is deduced from band assignments, **Table 1**. It can be seen that while all the MLCT peaks originate from transitions from the $d\pi$ orbital on Ru^{II} to π^* on bpy, the assignment is more complicated for the excitations with lower wavelength. For the **n2** polymer, for example, the peak at 234 nm derives mainly from transitions of $\pi \rightarrow \pi^*$ on the bridge or bpy ligands, and the peak at 260 nm has a mix of bridge to bpy $\pi \rightarrow \pi^*$, bpy to bpy $\pi \rightarrow \pi^*$, and also some MLCT character. There are almost no differences in the calculated spectra between the three polymers with and without the linker, as is also found experimentally.⁹ The MLCT peaks arising from the excitation of Ru $d\pi$ electron to bpy π^* orbitals do not correspond to HOMO-LUMO transitions in almost all instances. Instead, these MLCT excitations peaks derive from other higher-lying occupied states (i.e. HOMO-2) that are localized on Ru to LUMO because of the attached linker group. Also, since HOMO is located on the bridge in most pendants, and it has no spatial overlap with LUMO (which is localized on the bpy ligand), we find that most excitations do not involve HOMO.

Conclusions

We investigated how the polymer dynamics influences optical and electronic properties of individual $[\text{Ru}(\text{bpy})_3]^{2+}$ complexes that are covalently attached to a polystyrene backbone with varying length of the covalent linker. These metallo-polymeric chromophore assemblies have been experimentally synthesized, and they are considered promising as a flexible material for charge/exciton transport for solar-to-fuel applications. We employed a combination of classical molecular dynamics, semi-empirical and first-principles electronic structure calculations to a gain broad insight into optical and electronic properties of these statistically complex systems.

Our work shows that distributions of the electronic energy levels of these Ru complexes are quite broad and multi-peaked, and show a strong dependence on the linker group connecting the

complex to the polymer backbone. However, the broad energy distribution does not stem from internal structural changes within these Ru complexes but rather from non-covalent interaction of the Ru complex with the linker group. The calculations show that HOMO and HOMO-1 states are mostly localized on the linker group rather than on the Ru complex itself, and the Ru-localized state closest to the energy gap is HOMO-2 in the acetonitrile-solvated systems considered here. Both semi-empirical and DFT calculations consistently show this general feature.

Regardless of the specific ordering of these Ru-localized states with respect to the linker-localized states, there exist several general trends in the energy distribution. In case of the polymer assembly with the shortest linker (**n0** polymer), the energy distributions show a bimodal distribution for the LUMO while the other two polymers with longer linkers do not show such bimodal distribution of the energy levels. Our calculations show that each Ru pendant (Ru complex + linker) yields one of the two bimodal peaks but not both. For efficient hole transport through $[\text{Ru}(\text{bpy})_3]^{2+}$ complexes, it is essential that all Ru-localized states span a similar energy range so that none of these electronic states behave as a trap state for the hole. We observed that all the individual $[\text{Ru}(\text{bpy})_3]^{2+}$ pendants in the **n1** polymer yield a similar energy range (~ 0.5 eV) unlike the **n0** and **n2** polymers, and therefore the **n1** polymer could be the most desirable synthetic target from the electronic structure viewpoint. However, if the hole hopping is not efficient, then the hole would be trapped in the HOMO state, which is localized on the linker although HOMO is not involved in the prominent MLCT excitation of Ru-complexes because of the negligible spatial overlap between HOMO and LUMO. For the optical properties, the intrinsic MLCT excitation was found to be rather insensitive to the polymer dynamics regardless of the linker length. In particular, the lowest excitation peaks with MLCT character for all the polymers are the same as those of isolated $[\text{Ru}(\text{bpy})_3]^{2+}$ complex by itself. Because of the insignificant spatial overlap of HOMO (localized on the linker group) and LUMO (localized on bpy ligand on Ru complex),

	220 nm	234 nm	260 nm	380 nm
n0 with linker		$\pi\pi(\text{bridge}) \rightarrow \pi^*$ (bridge) $\pi\pi(\text{bpy}) \rightarrow \pi^*$ (bpy) $d\pi(\text{Ru}) \rightarrow \pi^*$ (bpy) $d\pi(\text{Ru}) \rightarrow \pi^*$ (bridge)	$d\pi(\text{Ru}) \rightarrow \pi^*$ (bpy) $\pi\pi(\text{bridge}) \rightarrow \pi^*$ (bpy)	$d\pi(\text{Ru}) \rightarrow \pi^*$ (bpy)
n1 with linker		$\pi\pi(\text{bridge}) \rightarrow \pi^*$ (bridge) $d\pi(\text{Ru}) \rightarrow \pi^*$ (bpy)	$\pi\pi(\text{bpy}) \rightarrow \pi^*$ (bpy) $d\pi(\text{Ru}) \rightarrow \pi^*$ (bpy)	$d\pi(\text{Ru}) \rightarrow \pi^*$ (bpy)
n2 with linker		$\pi\pi(\text{bridge}) \rightarrow \pi^*$ (bridge) $d\pi(\text{Ru}) \rightarrow \pi^*$ (bpy)	$\pi\pi(\text{bridge}) \rightarrow \pi^*$ (bpy) $\pi\pi(\text{bpy}) \rightarrow \pi^*$ (bpy) $d\pi(\text{Ru}) \rightarrow \pi^*$ (bpy)	$d\pi(\text{Ru}) \rightarrow \pi^*$ (bpy)
No linker = $[\text{Ru}(\text{bpy})_3]^{2+}$	$\pi\pi(\text{bpy}) \rightarrow \pi^*$ (bpy)		$d\pi(\text{Ru}) \rightarrow \pi^*$ (bpy)	$d\pi(\text{Ru}) \rightarrow \pi^*$ (bpy)

Table 1. Band assignments from the INDO/s calculated electronic spectra for the strongest peaks in **Fig. 8**, for pendants with and without linkers.

HOMO-LUMO transition does not appear in the electronic excitation. Instead, the most dominant contribution of MLCT character derives from the single-particle excitation of HOMO-2 and other Ru-localized states to LUMO. In this work, we did not consider the influence of different solvents on the electronic energy levels and excitation spectrum, and a future study will address these aspects, which are relevant for interpreting experimental measurements employing different types of polar and non-polar solvents.

Acknowledgements

This material is based upon work solely supported as part of the UNC EFRC: Center for Solar Fuels, an Energy Frontier Research Center funded by the U.S. Department of Energy, Office of Science, Office of Basic Energy Sciences under Award Number DE-SC0001011. We thank National Energy Research Scientific Computing Center, which is supported by the Office of Science of the U.S. Department of Energy under contract No. DE-AC02-05CH11231 for computational resources.

References

- Lewis, N. S.; Nocera, D. G., Powering the Planet: Chemical Challenges in Solar Energy Utilization. *Proceedings of the National Academy of Sciences of the United States of America* **2006**, *103* (43), 15729-15735.
- Maeda, K.; Domen, K., Photocatalytic Water Splitting: Recent Progress and Future Challenges. *J. Phys. Chem. Lett.* **2010**, *1* (18), 2655-2661.
- Concepcion, J. J.; House, R. L.; Papanikolas, J. M.; Meyer, T. J., Chemical approaches to artificial photosynthesis. *Proc. Nat. acad. Sci.* **2012**, *109* (39), 15560-15564.
- Nocera, D. G., The artificial leaf. *Acc. Chem. Res.* **2012**, *45* (5), 767-76.
- Faunce, T.; Styring, S.; Wasielewski, M. R.; Brudvig, G. W.; Rutherford, A. W.; Messinger, J.; Lee, A. F.; Hill, C. L.; deGroot, H.; Fontecave, M.; MacFarlane, D. R.; Hankamer, B.; Nocera, D. G.; Tiede, D. M.; Dau, H.; Hillier, W.; Wang, L.; Amal, R., Artificial photosynthesis as a frontier technology for energy sustainability. *Energy Environ. Sci.* **2013**, *6* (4), 1074-1076.
- House, R. A.; Bonino, C.; Hoertz, P.; Trainham, J.; Meyer, T., *pv magazine* **2013**.
- (a) Hagfeldt, A.; Boschloo, G.; Sun, L.; Kloo, L.; Pettersson, H., Dye-Sensitized Solar Cells. *Chem. Rev.* **2010**, *110* (11), 6595-6663; (b) Song, W.; Chen, Z.; Glasson, C. R. K.; Hanson, K.; Luo, H.; Norris, M. R.; Ashford, D. L.; Concepcion, J. J.; Brennaman, M. K.; Meyer, T. J., Interfacial Dynamics and Solar Fuel Formation in Dye-Sensitized Photoelectrosynthesis Cells. *ChemPhysChem* **2012**, *13* (12), 2882-2890.
- Wang, L.; Puodziukynaite, E.; Grumstrup, E. M.; Brown, A. C.; Keinan, S.; Schanze, K. S.; Reynolds, J. R.; Papanikolas, J. M., Ultrafast Formation of a Long-Lived Charge-Separated State in a Ru-Loaded Poly(3-hexylthiophene) Light-Harvesting Polymer. *J. Phys. Chem. Lett.* **2013**, *4* (14), 2269-2273.
- Fang, Z.; Ito, A.; Keinan, S.; Chen, Z.; Watson, Z.; Rochette, J.; Kanai, Y.; Taylor, D.; Schanze, K. S.; Meyer, T. J., Atom Transfer Radical Polymerization Preparation and Photophysical Properties of Polypyridylruthenium Derivatized Polystyrenes. *Inorg. Chem.* **2013**, *52* (15), 8511-8520.
- Fleming, C. N.; Maxwell, K. A.; DeSimone, J. M.; Meyer, T. J.; Papanikolas, J. M., Ultrafast Excited-State Energy Migration Dynamics in an Efficient Light-Harvesting Antenna Polymer Based on Ru(II) and Os(II) Polypyridyl Complexes. *J. Am. Chem. Soc.* **2001**, *123* (42), 10336-10347.
- Puodziukynaite, E.; Wang, L.; Schanze, K. S.; Papanikolas, J. M.; Reynolds, J. R., Poly(fluorene-co-thiophene)-based ionic transition-metal complex polymers for solar energy harvesting and storage applications. *Polymer Chemistry* **2014**, *5* (7), 2363-2369.
- Thompson David, W.; Ito, A.; Meyer Thomas, J., [Ru(bpy)₃]²⁺* and other remarkable metal-to-ligand charge transfer (MLCT) excited states. In *Pure Appl. Chem.*, 2013; Vol. 85, p 1257.
- Hatcher, E.; Balaeff, A.; Keinan, S.; Venkatramani, R.; Beratan, D. N., PNA versus DNA: Effects of Structural Fluctuations on Electronic Structure and Hole-Transport Mechanisms. *J. Am. Chem. Soc.* **2008**, *130* (35), 11752-11761.
- Venkatramani, R.; Keinan, S.; Balaeff, A.; Beratan, D. N., Nucleic Acid Charge Transfer: Black, White and Gray. *Coord. Chem. Rev.* **2011**, *255* (7-8), 635-648.
- Tummala, N. R.; Mehraeen, S.; Fu, Y.-T.; Risko, C.; Brédas, J.-L., Materials-Scale Implications of Solvent and Temperature on [6,6]-Phenyl-C61-butyric Acid Methyl Ester (PCBM): A Theoretical Perspective. *Advanced Functional Materials* **2013**, *23* (46), 5800-5813.
- Rappe, A. K.; Casewit, C. J.; Colwell, K. S.; Goddard, W. A.; Skiff, W. M., UFF, a full periodic table force field for molecular mechanics and molecular dynamics simulations. *J. Am. Chem. Soc.* **1992**, *114* (25), 10024-10035.
- Becke, A. D., *J. Chem. Phys.* **1992**, *96* (2155).
- Hay, P. J.; Wadt, W. R., LACVP. *J. Chem. Phys.* **1985**, *82*, 299.
- Wadt, R. W.; Hay, P. J., *J. Chem. Phys.* **1985**, *82*, 284.
- Frisch, M. J. T., G. W.; Schlegel, H. B.; Scuseria, G. E.; Robb, M. A.; Cheeseman, J. R.; Montgomery, J. A., Jr.; Vreven, T.; Kudin, K. N.; Burant, J. C.; Millam, J. M.; Iyengar, S. S.; Tomasi, J.; Barone, V.; Mennucci, B.; Cossi, M.; Scalmani, G.; Rega, N.; Petersson, G. A.; Nakatsuji, H.; Hada, M.; Ehara, M.; Toyota, K.; Fukuda, R.; Hasegawa, J.; Ishida, M.; Nakajima, T.; Honda, Y.; Kitao, O.; Nakai, H.; Klene, M.; Li, X.; Knox, J. E.; Hratchian, H. P.; Cross, J. B.; Bakken, V.; Adamo, C.; Jaramillo, J.; Gomperts, R.; Stratmann, R. E.; Yazyev, O.; Austin, A. J.; Cammi, R.; Pomelli, C.; Ochterski, J. W.; Ayala, P. Y.; Morokuma, K.; Voth, G. A.; Salvador, P.; Dannenberg, J. J.; Zakrzewski, V. G.; Dapprich, S.; Daniels, A. D.; Strain, M. C.; Farkas, O.; Malick, D. K.; Rabuck, A. D.; Raghavachari, K.; Foresman, J. B.; Ortiz, J. V.; Cui, Q.; Baboul, A. G.; Clifford, S.; Cioslowski, J.; Stefanov, B. B.; Liu, G.; Liashenko, A.; Piskorz, P.; Komaromi, I.; Martin, R. L.; Fox, D. J.; Keith, T.; Al-Laham, M. A.; Peng, C. Y.; Nanayakkara, A.; Challacombe, M.; Gill, P. M. W.; Johnson, B.; Chen, W.; Wong, M. W.; Gonzalez, C.; Pople, J. A., Gaussian 03, revision C.02, Gaussian, Inc.: Wallingford, CT, 2004.
- Ridley, J.; Zerner, M., INDO. *Theor. Chim. Acta* **1973**, *32*, 111.
- Zeng, J.; Hush, N. S.; Reimers, J. R., CNDO - Solvent effects on molecular and ionic spectra. VII: Modeling the absorption and electroabsorption spectra of pentaammineruthenium(II)-pyrazine and its conjugate acid in water. *J. Am. Chem. Soc.* **1996**, *118*, 2059.
- Gorelsky, S. I.; Lever, A. B. P., Electronic structure and spectra of ruthenium diimine complexes by density functional theory and INDO/S. Comparison of the two methods. *Journal of Organometallic Chemistry* **2001**, *635* (1-2), 187-196.
- Gorelsky, S. I.; Lever, A. B. P.; Ebadi, M., Ruthenium d-orbital delocalization in bis(bipyridine)ruthenium derivatives of redox active quinonoid ligands. *Coord. Chem. Rev.* **2002**, *230* (1-2), 97-105.

25. McMahon, D. P.; Cheung, D. L.; Goris, L.; Dacuña, J.; Salleo, A.; Troisi, A., Relation between Microstructure and Charge Transport in Polymers of Different Regioregularity. *J. Phys. Chem. C* **2011**, *115* (39), 19386-19393.